UNCERTAINTY OF TILTED IRRADIANCE MEASUREMENTS USING PHOTODIODES AND REFERENCE CELLS

Anton Driesse[1], Stefan Wilbert[2], Anne Forstinger[3]

[1] PV Performance Labs, Emmy-Noether-Str. 2, Freiburg, Germany,
anton.driesse@pvperformancelabs.com

[2]German Aerospace Center (DLR), Almeria, Spain
[3]CSP Services GmbH, Cologne, Germany

Irradiance is one of the most important parameters for the solar industry. However, it is very challenging to measure accurately, therefore it is all the more important to quantify the uncertainty of irradiance measurements. Current best practices tend to use worst-case assumptions and apply them more-or-less uniformly, possibly leading to overly pessimistic uncertainty evaluations. In this work we evaluate the uncertainty of individual tilted irradiance measurements of time series data using two different approaches: first, we compare the measurements from five different devices of each type operating in parallel for a GUM type A evaluation; and second, we calculate the uncertainty associated with several key properties of the instruments (spectral response, directional response, temperature response) and combine them in a GUM type B evaluation for comparison. Correlations seen between the A and B results in one year of data at two very different sites indicate that the second method should be suitable for uncertainty evaluations in other locations.

Keywords: Solar radiation, plane-of-array, uncertainty, pyranometer, reference cell, photodiode, spectral response, directional response, monitoring, system performance

1 INTRODUCTION

Solar irradiance measurements provide essential information at all stages of the PV system life cycle. Site selection, system design, certification, operation, maintenance, trouble-shooting, upgrading, expansion, and even decommissioning—all business decisions rely on accurate solar irradiance data. Most modern sensors used to measure global (or hemispherical) solar irradiance fall into three broad categories: thermopile pyranometers, photodiode pyranometers, and photovoltaic reference cells, and within these categories are instruments in various price and accuracy classes. While irradiance measured with pyranometers and reference cells are two fundamentally different quantities, the users of both instrument categories share the same need to understand the uncertainty of their measurements.

In this work we evaluate the uncertainty of individual tilted irradiance measurements in time series data using two different approaches based on [1] and [2]: first, we compare the measurements from five different devices of each type operating in parallel for a GUM type A evaluation; and second, we calculate the uncertainty associated with several key properties of the instruments (spectral response, directional response, temperature response) and combine them in a GUM type B evaluation. In this manner we obtain two estimates for the uncertainty of each measurement in each time series. The aim is to validate the type B approach at two locations for which such data is available, and thereby demonstrate that the type B method is suitable for uncertainty evaluations in other locations.

Realistic assessments of uncertainty substantially increase the usefulness and value of irradiance measurements. Not only can they be helpful in quality control procedures, for example to identify outliers, but they are essential inputs to determine uncertainties of key performance indicators (KPI), or uncertainties of aggregate values.

2 METHOD

As mentioned in the introduction, this work evaluates measurement uncertainties for two categories of sensors using two methods and data from two locations. The two categories, photodiode pyranometers and PV reference cells, are each represented by five products as listed in **Table 1**. Outdoor operating data were collected in Freiburg, Germany and Albuquerque, USA, and relevant instrument properties were measured by JRC Ispra and PV Performance Labs, Freiburg. The latter are described in more detail in [3] and [4].

Table 1 Sensor identification

Manufacturer	Model	Category
Apogee Instruments	SP-110	Photodiode pyranometer
Eko Instruments	ML-01	
Kipp & Zonen	SP-Lite2	
LI-COR	LI-200	
Skye Instruments	SKS-1110	
EETS	RC01	Reference cell
Fraunhofer ISE	11311102	
Ingenieurbuero Mencke & Tegtmeyer (IMT)	SiS-02-Pt100	
	Si-02-Pt100	
NES - Mess- und Meldesysteme	SOZ-03	

There are multiple differences between these product categories, but one is particularly important for the uncertainty analysis: the measurand for the photodiode pyranometer is clearly defined as the broadband hemispherical irradiance incident on the measurement plane, whereas the measurand for the reference cells lacks such a precise definition. Consequently, for the photodiodes the “true” value of the measurand can be estimated with superior thermal instruments (in our case even multiple instruments), whereas for the reference cells a substitute must be found. In this work we use the most practical

(although somewhat optimistic) estimate that the true value is the mean of the five instruments. These estimates of the true value are called *reference values* in the following, and deviations from the reference values are called *measurement errors*.

2.1 Type A evaluation based on multiple observations under the same conditions

Type A uncertainty evaluations use the observed dispersion of multiple measurements to infer a level of uncertainty. In this analysis the dispersion between simultaneous readings (one-minute average values) from five similar instruments is used to infer the level of uncertainty of measurements using an *arbitrary instrument* in the category. This is a suitable objective as for average users the instruments in a certain category or class are more or less equivalent.

Measurement errors are calculated as the difference from the reference values (as discussed above), and the sample standard deviation (std) of these five errors is normally adopted as the standard uncertainty (k=1). Since the number of readings is small and the normality of their distribution unproven, alternate approaches could be considered.

In the case of the photodiodes the mean of the five readings usually differs from the thermopile reference value, which represents a bias that is not reflected in the standard deviation alone. Therefore, the bias is treated like an additional source of uncertainty and combined with the sample standard deviation as the root of the sum of squares (RSS):

$$u = \sqrt{std^2 + bias^2} \quad (1)$$

Since the reference value for the reference cells is chosen to be their mean value, the bias is always zero and the uncertainty is estimated only by the sample standard deviation.

2.2 Type B evaluation based on a priori knowledge about input quantities

The aim of the second evaluation is to quantify the separate sources of uncertainty that contribute in the overall uncertainty individually, and combine them using the standard rules of the GUM and the measurement equation. The measurement equation describes how the measurand is calculated from the instrument's output signal, which is a small voltage for these 10 irradiance sensors.

Table 2 (located near the end of this article) lists and describes the main characteristics that influence the instruments. The table also makes clear that some additional information is needed to complete the uncertainty estimates, such as sun angles and air temperature, but by far the most complex of these is spectral irradiance. We will discuss this point next since it is central to the measurement equation that will follow.

2.3 Uncertainty of spectral mismatch

Differences between device spectral responses and the ideal or reference spectral response lead to measurement errors, called spectral mismatch errors. These errors (and likewise the uncertainty associated with them) depend on the spectrum of the incident irradiance. Therefore, spectral irradiance is a required input for the type B method.

Since spectral irradiance measurements are usually unavailable, the spectral irradiance must be simulated for all possible sky conditions. The SEDES2 algorithm is one of the few options available for this task, and is used for example in [5]. We choose a different approach here motivated by the observation that the simulated spectra do not need to be completely accurate: only the correct spectral mismatch factors are needed. The chosen solution uses a clear-sky spectrum simulated using SMARTS2 [6] to estimate the SMM for all times when beam irradiance is "strong", which means clear-sky index for beam irradiance is greater than 0.5. We call these conditions "open-sky". At other times when the sun is obscured by clouds SMM is not calculated at all, but rather a simple empirical relationship is used to estimate its uncertainty.

The clear-sky assumption is tested using tilted spectral irradiance measurements and simulations in Freiburg, Germany (30° tilt) and Golden, Colorado (40° tilt) [7]. **Figure 1** and **Figure 2** show the SMM calculated using the average photodiode spectral response at the Colorado location, highlighting the values for summer (red), winter (blue), and behind plane of array (black).

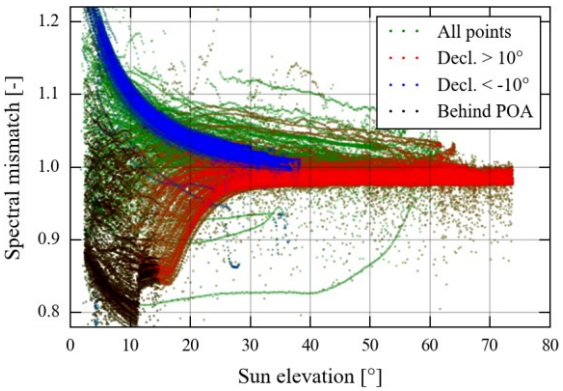

Figure 1 Spectral mismatch for the average photodiode from measured spectra (350-1050 nm) in Golden, CO.

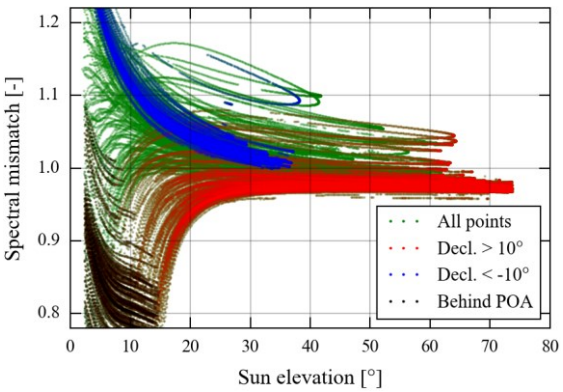

Figure 2 Spectral mismatch for the average photodiode from clear-sky simulated spectra (350-1050 nm) in Golden, CO.

The similarity between the SMM from measured and simulated spectral data is visually striking and indeed the histogram in **Figure 3** shows that the differences are most often quite small. Nevertheless, at higher sun elevations there is a distinct negative bias of a 1-2% on the SMM from simulations which is not seen in the second location, Freiburg. This could be due to the source atmospheric

data (CAMS global reanalysis [8]), incorrect assumptions about the local or zonal albedo, or limitations of the SMARTS model itself. Similar analysis for the photodiodes in Freiburg, as well as for the reference cells in both locations showed SMM values generally somewhat closer to unity, and consequently also slightly smaller deviations than shown in **Figure 3**.

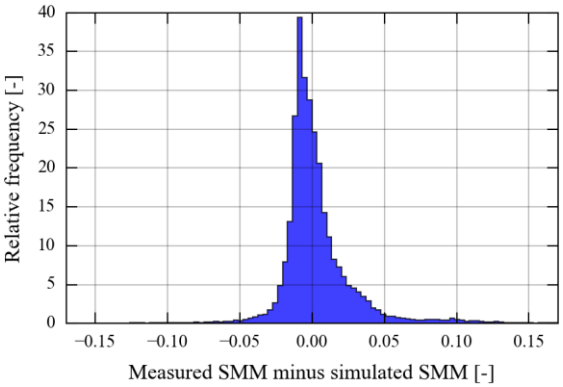

Figure 3 Differences between the SMM from measured and simulated spectra for the average photodiode in Golden, CO.

The identification of open-sky conditions is generally easy because intermediate DNI conditions occur much less frequently than low or high. Furthermore, high DNI conditions usually account for a large portion of the total annual energy (> 75% in Freiburg during the period of the data), thus being able to predict the spectral mismatch factor for 75% of the available energy is a valuable capability on its own. Further validation for additional climate zones should be carried out for general application of this mismatch prediction method, but since the two validation locations are similar to our two irradiance sensor locations we proceed to use it here for the uncertainty analysis.

To estimate uncertainty due to SMM, we calculate the SMM for each of the five sensors in each group, determine the SMM error by subtracting the reference value (which is 1.0 in the case of the photodiodes, and the mean of five for the reference cells), and finally combine the mean and standard deviation of the errors using (1).

2.4 The measurement equation

The required measurement equation is developed beginning with the most basic equation possible, which defines a linear relationship between the irradiance G, the measured signal V via the calibration factor or responsivity R_0:

$$G_{m,basic} = \frac{V}{R_0} \tag{2}$$

This basic equation is standard for photodiode measurements. However photovoltaic devices usually exhibit a linear temperature dependency that increases the apparent responsivity at higher temperatures. Thus a temperature correction can be incorporated into the measurement equation as follows:

$$G_{m,tc} = \frac{V}{R_0(1+\alpha(T-25))} \tag{3}$$

where α is the unit-less linear temperature coefficient and T is the instrument temperature in °C. This equation is usually recommended for use with reference cells and is frequently implemented in the electronics of powered reference cell products, where a typical value for α is 500 ppm. If the value of α for a photodiode is known, this equation can also be used for temperature correction of photodiode measurements.

Additional characteristics of sensors can be expressed in general as a function f_R that modifies the original responsivity R_0:

$$G_m = \frac{V}{R_o \cdot f_R(\vec{C},\vec{P}) \cdot (1+\alpha(T-25))} \tag{4}$$

where C and P are vectors of measurement conditions and sensor properties (characteristics) respectively. When included in the measurement equation this responsivity modification serves as a correction and in general improves the accuracy of the measured irradiance. (It should be noted here that the temperature correction could also be placed within the modifier function but is retained in its usual place for familiarity.)

To incorporate directional response characteristics or incidence angle modifier (IAM) into the measurement equation a separation of beam and diffuse irradiance is needed, which is done via the beam fraction, f_{beam}:

$$f_R = \begin{bmatrix} f_{beam} \cdot IAM_{beam}(\theta) + \\ (1-f_{beam}) \cdot IAM_{diff}(\beta) \end{bmatrix} \tag{5}$$

For the open sky case the spectral mismatch is likewise calculated separately for beam and diffuse irradiance, but the two must be immediately combined into a single global SMM_{clear}. This is because the SMM for beam and diffuse vary much more strongly than the combined SMM for global irradiance, and this individual variability should not feed into the uncertainty assessment for global irradiance. The new modifier function is thus:

$$f_R = \begin{bmatrix} f_{beam} \cdot IAM_{beam}(\theta) + \\ (1-f_{beam}) \cdot IAM_{diff}(\beta) \end{bmatrix} \cdot SMM_{clear} \tag{6}$$

which can be written more compactly as:

$$f_R = IAM_{clear}(f_{beam},\theta,\beta) \cdot SMM_{clear} \tag{7}$$

Similarly for sky conditions without beam irradiance the responsivity modifier would be:

$$f_R = IAM_{diff}(\beta) \cdot SMM_{variable} \tag{8}$$

These last two equations are blended by using a new factor f_{open} which varies between zero and one, just like f_{beam}:

$$f_R = \begin{bmatrix} f_{open} \cdot IAM_{clear}(f_{beam},\theta,\beta) \cdot SMM_{clear} \\ +(1-f_{open}) \cdot IAM_{diff}(\beta) \cdot SMM_{variable} \end{bmatrix} \tag{9}$$

The value of f_{open} is obtained by applying a simple clipping or sigmoid function to the clearness index for beam irradiance. And finally the non-linearity (NLIN) is appended as a function of the measured voltage:

$$f_R = \begin{bmatrix} f_{open} \cdot IAM_{clear}(f_{beam},\theta,\beta) \cdot SMM_{clear} \\ +(1-f_{open}) \cdot IAM_{diff}(\beta) \cdot SMM_{variable} \end{bmatrix} \cdot NLIN(V) \tag{10}$$

With this responsivity modifier substituted into equation (4) it is possible to implement correction functions. More importantly for this work, however, the equation defines the propagation path from uncertainties in the

inputs (both operating conditions and sensor properties) and uncertainty in the output: the measured irradiance. Even if measured irradiance is calculated without corrections using the most basic equation (2), the combination of equations (4) and (10) is needed to calculate the type B uncertainty of that measured irradiance.

It should be stressed that not all sources of uncertainty are included in these calculations. Possible bias due to incorrect calibration factors was removed by applying a scaling factor to the measurements of each instrument, which is essentially a post-calibration. This was done using stable irradiance values in the range 800–1100 W/m^2 at times and angle of incidence less than 5°. Furthermore, the instruments were aligned with great care and cleaned frequently, usually twice per week. Finally, the comparisons between sensors are relative measurements, therefore logger calibration errors cancel out. A complete uncertainty analysis for field measurements with these instruments should include additional allowance for uncertainty due to calibration, alignment, soiling, aging, data logger and perhaps other installation-specific factors, and the combined uncertainty would be larger than those shown in this paper.

The propagation of uncertainties through this equation is not simple and is therefore not done analytically as shown in [2]. Instead, the open-source software package *uncertainties* [9] is used, which calculates all the required partial derivatives internally. Hence we can proceed directly from the descriptions of methods and inputs to results.

3 RESULTS AND DISCUSSION

After calculating the uncertainties using the two methods we need to evaluate their similarity. A key aspect of the measurement uncertainty is its time-varying nature due to fluctuating operating conditions. For solar energy applications such fluctuations are often visualized in the form of sun-path diagrams, where each pixel represents the mean value of a parameter for all times where the sun occupied that position in the sky. We will therefore show a small selection of sun-path diagrams depicting some general observations, followed by more direct comparisons.

Non-linear linearity is by far the smallest of the effect considered, and as shown in **Figure 4** it manifests itself primarily at low irradiance. The uncertainty due to temperature response (**Figure 5**) is somewhat higher, and is greatest in winter, with a slight lean towards morning for photodiodes. For reference cells this seasonal trend is inverted since it is in the hot summer that operating temperatures are furthest from the reference temperatures, but overall the uncertainty level is lower because a temperature correction is always done. Directional response uncertainty in **Figure 6** overshadows the previous two, and as the angle of incident approaches 90°, the uncertainty of the angle itself further accentuates the uncertainty of the IAM. Over most of the angular range reference cells have lower uncertainty, primarily because they are compared to their mean value, and not to the Lambertian ideal. The final example in **Figure 7** shows the uncertainty due to spectral mismatch obtained using the clear-sky spectral simulations. Once again reference cells have the benefit of being compared to each other, and their uncertainty due to SMM using clear-sky spectra lies below 1% almost always.

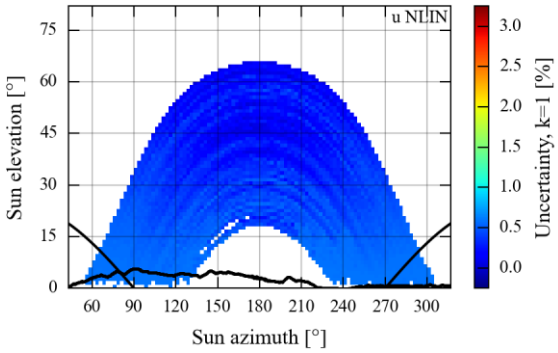

Figure 4 The uncertainty contribution of non-linearity using the example of photodiodes in Freiburg.

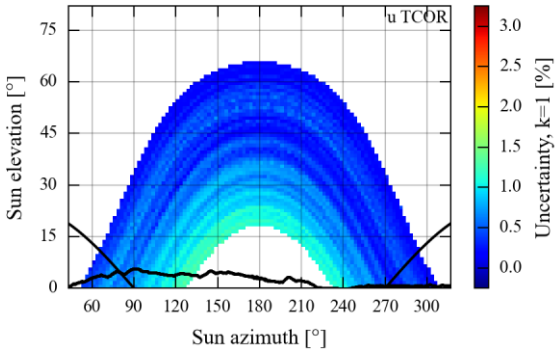

Figure 5 The uncertainty contribution of temperature response using the example of photodiodes in Freiburg.

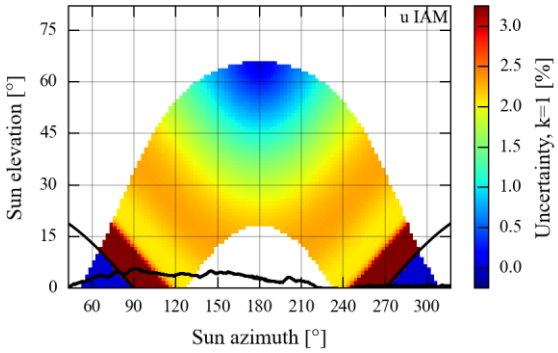

Figure 6 The uncertainty contribution of directional response using the example of photodiodes in Freiburg.

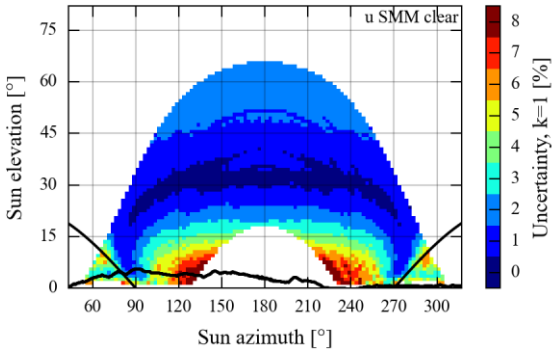

Figure 7 The uncertainty contribution of spectral response for open-sky conditions using the example of photodiodes in Freiburg.

The final two sun path diagrams (**Figure 8** and **Figure 9**) show the full type A and type B uncertainties for photodiodes under all sky conditions in Freiburg. Many matching trends and patterns can be seen in these diagrams, which is a first indication that the type B procedure described in this paper is indeed capable of producing a very plausible and realistic uncertainty profile. However, this is the best of four cases considered. Some challenges of the other three cases will be seen more clearly in other graphical representations.

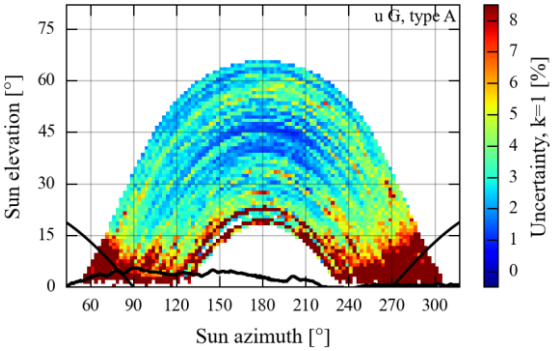

Figure 8 The time-dependent uncertainty of photodiode irradiance measurements in Freiburg estimated from measurement errors w.r.t a broadband reference.

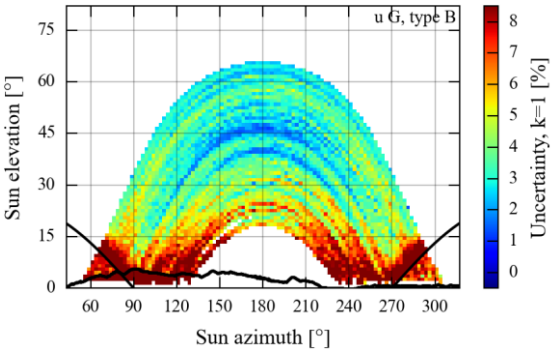

Figure 9 The time-dependent uncertainty of photodiode irradiance measurements in Freiburg estimated by combining multiple component sources of uncertainties.

While these sun-path diagrams provide useful insights, a more compact and direct comparison is the traditional scatter plot of Type B vs. Type A. These are shown in **Figure 10** (located near the end of this article). For photodiodes, (a) and (b), there is a clear correlation between the two uncertainty estimates albeit with some overestimation in the type B. Uncertainties reach substantially higher values in Albuquerque (b) which is due at least in part to the higher mismatch factors at high irradiance at that location. This is a group bias that propagates into the overall type B uncertainty. The type A estimate picks up the same effect through higher deviations from the broadband reference irradiance.

For the reference cells, (c) and (d), the correlation during non-open-sky conditions is more clearly visible than for the open-sky conditions. In fact, for open-sky conditions the clearest feature is the substantial overestimation of type B. The lack of correlation here is rooted in the non-normal distribution of the characteristics of the five products, in particular the directional responses.

Finally, we go back to the measurements of each individual sensor to evaluate whether they reflect the expectations implied by the calculated uncertainty. For example, when an uncertainty u (k=1) is given, the expectation is that roughly 68% of the measurements will have an error less than u, and 95% will have an error of less than $2u$ (k=2). The final four charts in **Figure 11** plot the CDF of the measurement errors for each individual instrument divided by the estimated uncertainty in order to assess this aspect. For the photodiodes, (a) and (b), the shapes and position of the CDF are not far from the Gaussian dotted line, indicating that the measurement errors are in line with expectations: i.e. for most products more than 68% of the errors were smaller than the k=1 uncertainty level, and similarly for most products more than 95% of the errors were smaller than the expanded k=2 uncertainty. Overall the five photodiodes do not differ substantially and it appears appropriate to use the same type B uncertainty estimate for all.

For the reference cells, (c) and (d), the picture differs substantially. The uncertainty estimates for the group are much too high for three of the cells, and too low for the other two. Reference cell errors are calculated with respect to the mean of the group and the separation in this diagram highlights the fact that deviations from the mean are more systematic than random. Consequently, the type B uncertainty estimate calculated for the group is not appropriate for any of the members of the group.

4 CONCLUSIONS

The dual uncertainty analysis carried out in this work produced consistent uncertainty estimates for the group of five photodiodes in two very different locations. This paves the way for using the more flexible type B method to estimate tilted measurement uncertainty for arbitrary photodiode pyranometers at arbitrary locations and in arbitrary orientations. Nevertheless, some caution—and preferably additional validation—would be recommended for use in more extreme climates and measurement situations.

For the group of five reference cells the same consistency could not be observed because the group contained two units having unique designs and operating characteristics. Thus, uncertainty estimates suitable for all five members of the group could not be determined. This is not a failure of the method as such, but rather a consequence of a problem with the input.

A more fundamental obstacle to estimating the uncertainty for reference cells is the lack of a precise definition of the measurand, or alternatively of the required instrument characteristics. While there are legitimate reasons for having reference cells with different characteristics for different purposes, each needs a standardized definition against which measurement errors and uncertainties can be gauged.

Although not apparent from the results shown in this paper, the strongest contributor to the uncertainty of photodiode measurements was by far the spectral mismatch. By contrast the reference cells demonstrated stronger variability in directional response. Another observation related to both of these aspects is that to calculate spectral mismatch on a tilted plane it is essential to consider the beam and diffuse spectral irradiance separately. They always differ strongly and must be mixed in the correct proportions.

The calculation steps that lead to the uncertainty estimates are complex, but much can be automated. In the context of low-cost sensors such calculations could be offered as a service to achieve economies of scale, or alternatively typical year uncertainty profiles could be generated in the form of look-up tables (LUT) as a one-time effort. The method is of course not inherently limited to use with low-cost sensors, but for thermopile pyranometers the spectral mismatch effect is generally so small that the large effort of simulating spectral irradiance can perhaps be spared.

Looking beyond uncertainty estimates, the approach of using clear-sky spectra to estimate spectral mismatch for a broader range of sky conditions holds promise for use in correction procedures for photodiodes pyranometers. But perhaps even more importantly, this approach could be used to estimate energy gains and losses in PV power plants due to spectral mismatch.

5 ACKNOWLEDGEMENTS

The authors thank the German Ministry for Economic Affairs and Energy for funding this study within the SOLREV project (contract number 03EE1010). We would also like to acknowledge the supporters and partners of the PVSENSOR project, which provided core data for this study—especially JRC Ispra and Sandia National Labs. We are also grateful to various organizations that made supporting data available, such as Fraunhofer ISE and the National Renewable Energy Lab.

6 AUTHOR CONTRIBUTIONS

Anton Driesse: Conceptualization, Data curation, Formal analysis, Methodology, Software, Validation, Visualization, Writing – original draft, Writing – review & editing. **Stefan Wilbert**: Conceptualization, Writing – review & editing. **Anne Forstinger**: Writing – review & editing.

7 REFERENCES

[1] Joint Committee for Guides in Metrology Working Group 1. “Guide to the Expression of Uncertainty in Measurement,” 2008.

[2] “ASTM G213-17 Standard Guide for Evaluating Uncertainty in Calibration and Field Measurements of Broadband Irradiance with Pyranometers and Pyrheliometers,” ASTM International, 2017. doi: 10.1520/G0213-17.

[3] A. Driesse and W. Zaaiman, “Characterization of Global Irradiance Sensors for use with PV Systems,” Proc. 42nd IEEE PVSC, 2015.

[4] A. Driesse et al., “Indoor and Outdoor Evaluation of Global Irradiance Sensors,” 30th EU-PVSEC, Hamburg, 2015.

[5] A. Forstinger et al “Uncertainty calculation method for photodiode pyranometers,” accepted for publication in Solar RRL, 2021.

[6] Gueymard, C.A., “SMARTS2, Simple Model of the Atmospheric Radiative Transfer of Sunshine: Algorithms and performance assessment,” Florida Solar Energy Center, 1995.

[7] A. Andreas and T. Stoffel, “NREL Solar Radiation Research Laboratory (SRRL): Baseline Measurement System (BMS),” Golden, Colorado, 1981, NREL Report No. DA-5500-56488, doi: 10.5439/1052221.

[8] A. Inness et al., “The CAMS reanalysis of atmospheric composition,” Atmos. Chem. Phys., vol. 19, no. 6, pp. 3515–3556, Mar. 2019, doi: 10.5194/acp-19-3515-2019.

[9] Eric O. Lebigot, “Uncertainties: a Python package for calculations with uncertainties”, version 3.1.6 https://pypi.org/ project/uncertainties/.

Table 2 Summary of the uncertainty components evaluated in the type B analysis.

Source of uncertainty	Details for photodiodes	Details for reference cells	Additional notes
Directional response or incidence angle modifier (IAM)	The ideal directional response is Lambertian. Uncertainty varies by angle and is estimated by the RSS of the standard deviation and bias at that angle. The IAM uncertainty for diffuse irradiance is 0.2%.	The ideal directional response is defined as the average directional response of the 5 devices at a given angle. Uncertainty varies by angle, and is estimated as the standard deviation of the responses at that angle. The IAM uncertainty for diffuse irradiance is 0.2%.	The uncertainty on the angle of incidence is 0.5°.
Spectral response, which leads to spectral mismatch (SMM)	The ideal mismatch factor is 1.0. The uncertainty varies by spectrum, and is estimated by the RSS of the standard deviation and bias under that spectrum for open-sky conditions.	The ideal mismatch is the average mismatch of the 5 devices under a given spectrum. The uncertainty varies by spectrum, and is estimated by the standard deviation of the 5 mismatch values under that spectrum for open-sky conditions.	For non-open-sky conditions the average mismatch is estimated at 1.0 and the uncertainty decreases as total POA irradiance increases.
Temperature response or correction (TCOR)	Signal is not adjusted for temperature. Assume a fictional α=0 for the measurement equation and use the measured ambient temperature. u_α = 500 ppm u_T= 4°C	Signal is already adjusted using the internal measured temperature T and factory-specified temperature coefficient α. The uncertainty is added with a second fictional adjustment with α=0. u_α = 80 ppm u_T= 1°C	Through the measurement equation this uncertainty grows as the temperature deviates further from 25 °C
Linearity or non-linearity (NLIN)	Some photodiodes show substantially higher non-linearity than reference cells. $u_{lin,max}$=0.6%	This is a negligible factor for most reference cells. $u_{lin,max}$=0.2%	This uncertainty is zero at 1000 W/m^2 and increases linearly away from this value to the maximum at 0 W/m^2
Calibration or normalization (CAL)	All measurements were scaled to produce the same reading at the standard reference conditions AM1.5G and 25 °C. u_{cal}=0.5%	All measurements were scaled to produce the same reading at the standard reference conditions AM1.5G and 25 °C. u_{cal}=0.5%	Since the reference conditions do typically not occur naturally, high irradiance conditions were used together with corrections for spectrum and temperature.
Datalogger (LOG)	The logger uncertainty is considered to be covered in the uncertainty of calibration/normalization.	The logger uncertainty is considered to be covered in the uncertainty of calibration/normalization.	The uncertainty of the logger used here is very small compared to other factors.

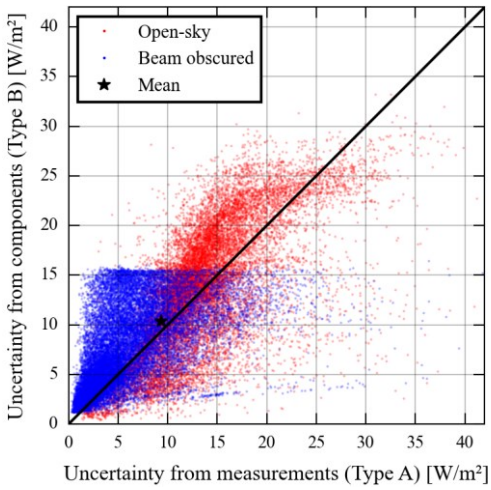

(a) Photodiodes in Freiburg

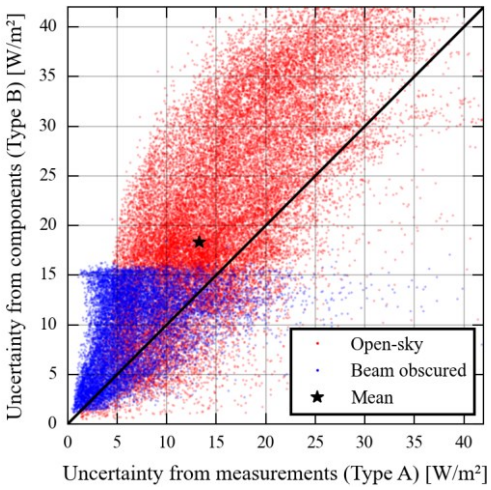

(b) Photodiodes in Albuquerque

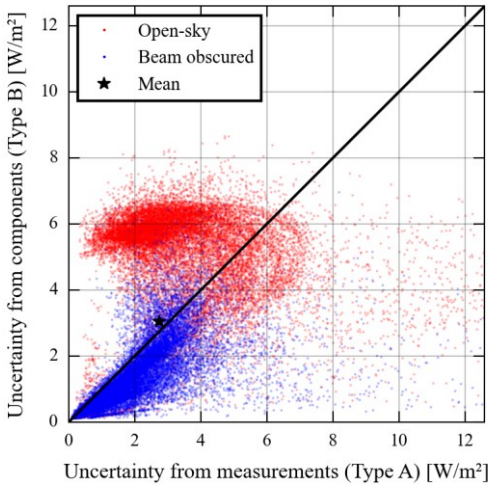

(c) Reference cells in Freiburg

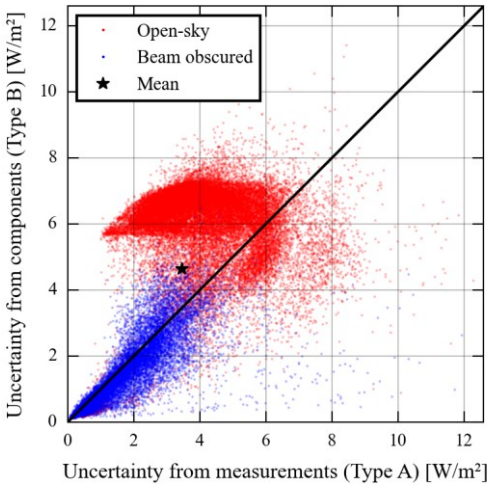

(d) Reference cells in Albuquerque

Figure 10 Scatter charts plotting the type B uncertainty estimates against the type A estimates. The uncertainties during open-sky conditions are shown in red. Note that the scale of the lower two graphs is only 30% of the upper graphs, reflecting the fact that the photodiodes are compared against a broadband reference whereas the reference cells are compared against the mean of the group.

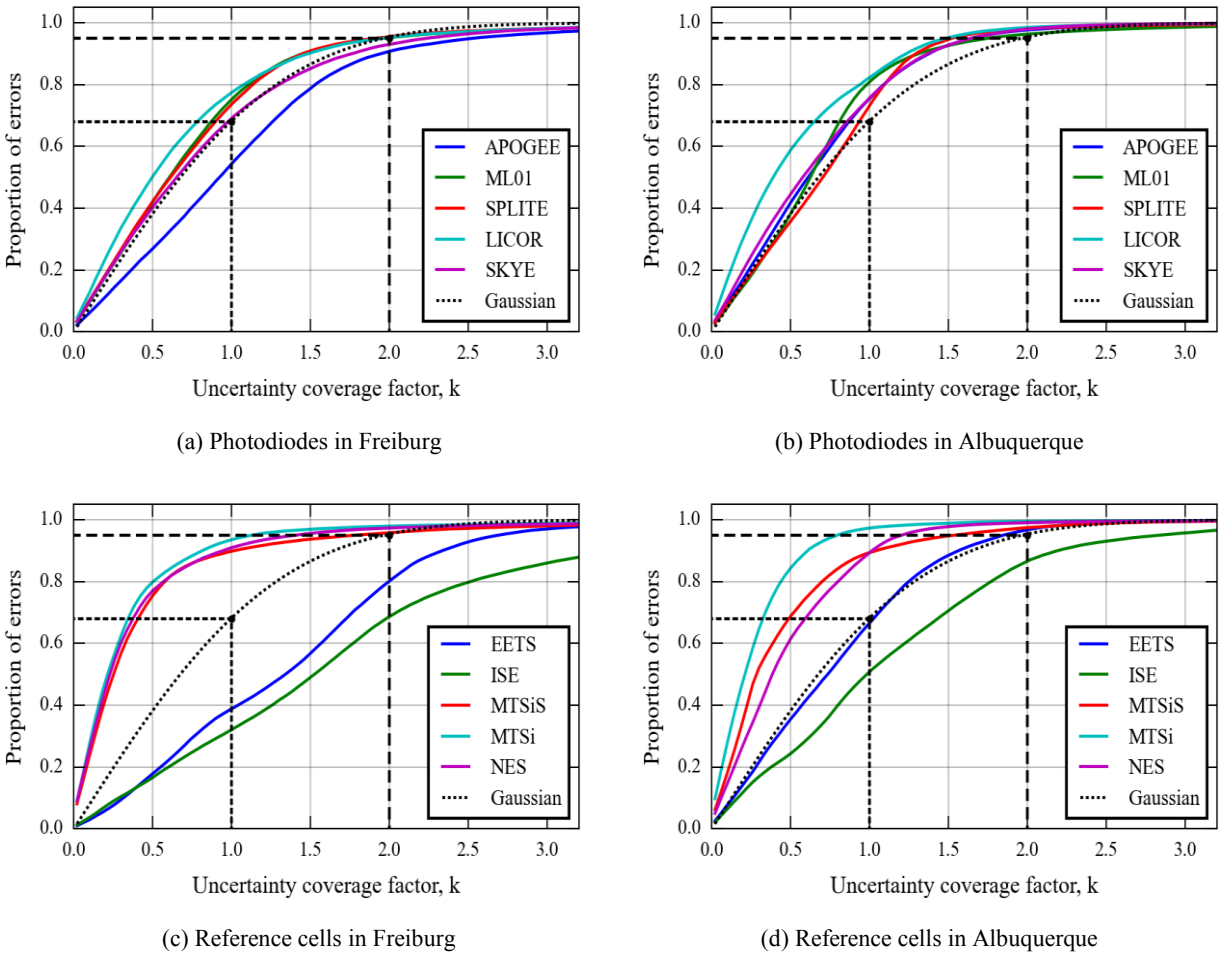

(a) Photodiodes in Freiburg

(b) Photodiodes in Albuquerque

(c) Reference cells in Freiburg

(d) Reference cells in Albuquerque

Figure 11 Cumulative distributions functions (CDF) of measurement errors normalized by the type B uncertainty estimates. When a curve lies above the dotted Gaussian line, the errors are smaller than expected based on the type B uncertainty estimates; when it lies below, the errors were larger than expected.